Soft Matter

PAPER

View Article Online
View Journal | View Issue

Cite this: *Soft Matter*, 2025, **21**, 1225

Electrically conducting porous hydrogels by a self-assembled percolating pristine graphene network†

Reihaneh Mohammadi Sejoubsari,[a] Thomas O. Xu,[a] Shawn P. Ward,[a] Nishadi M. Bandara,[a] Zhihao Zhang[b] and Douglas H. Adamson *[ab]

Received 6th November 2024,
Accepted 8th January 2025

DOI: 10.1039/d4sm01311e

rsc.li/soft-matter-journal

This study introduces a method for synthesizing electrically conductive hydrogels by incorporating a self-assembled, percolating graphene network. Our approach differs from previous approaches in two crucial aspects: using pristine graphene rather than graphene oxide and self-assembling the percolation network rather than creating random networks by blending. We use pristine graphene at an oil–water interface to stabilize a water-in-oil emulsion, successfully creating hydrogel foams with conductivities up to 15 mS m^{-1} and tunable porosity. Our approach avoids the need for the conductivity-degrading oxidation process to form GO and decreases the amount of graphitic filler needed for percolation, leading to superior mechanical properties. The concentration of monomer and graphite in the emulsion was optimized to control the cell size, stability, and swelling behavior of the final hydrogels, offering versatility in structure and functionality. Electrical conductivity and thermogravimetric analysis (TGA) confirmed the stability and conductive properties imparted by the graphene network. This method demonstrates a cost-effective route to conductive hydrogels, making them promising candidates for applications in sensors, energy storage, bioelectronics, and other advanced technologies.

Introduction

Hydrogels are hydrophilic, three-dimensional networks capable of absorbing large amounts of water, making them attractive for diverse applications such as sensing, drug delivery, and tissue engineering. Electrically conductive hydrogels (ECHs) are an advanced class of hydrogels that combine the water-retaining properties of traditional hydrogels with the ability to conduct electricity. This unique combination has enabled their use in various fields, including sensors,[1] fuel cells,[2] supercapacitors,[1] dye-sensitized solar cells,[3] and batteries.[4,5] However, there are challenges in making soft and flexible materials electrically conductive. Typical approaches[6] involve adding conductive fillers, using conductive polymers,[7–12] or relying on ionic conductivity.[13,14] Each approach has benefits and limitations, especially regarding mechanical properties[15] and biocompatibility.[16] We have addressed these challenges by incorporating a self-assembled graphene network within a poly(*N*-(hydroxymethyl) acrylamide) (PHMA) hydrogel.

Conductive fillers, such as metals, graphene oxide (GO), and carbon nanotubes (CNTs),[2,17,18] are commonly used to achieve conductivity. However, high filler loadings are often required to reach the percolation threshold, compromising the hydrogel's flexibility and softness. Moreover, these fillers can be limited by high cost, complex processing, and potential cytotoxicity concerns.[19] Among carbon-based fillers, graphite offers an attractive option. Unfortunately, pristine graphite is generally insoluble in water, requiring functionalization to ensure uniform dispersion, often at the expense of electrical conductivity and mechanical integrity.

In this study, we leverage the 2D surfactant properties of graphene to address this limitation by inducing the spontaneous exfoliation of graphite to graphene at an oil–water interface, where it stabilizes a water-in-oil emulsion. This method creates a self-assembled, conductive graphene network within a hydrogel matrix. Unlike conventional methods that require oxidative treatments or chemical modifications, our approach eliminates the need for chemical modification, allowing us to retain the properties of pristine graphite. This technique leads to a percolating graphene network in the hydrogel with minimal filler, maintaining the mechanical properties of the hydrogel.

Our exfoliation approach is driven by the reduction of the system's free energy when the oil and water phases are

[a] *Department of Chemistry, University of Connecticut, Storrs, Connecticut, USA. E-mail: Adamson@UConn.edu*
[b] *Polymer Program, Institute of Materials Science, University of Connecticut, Storrs, Connecticut, USA*

† Electronic supplementary information (ESI) available. See DOI: https://doi.org/10.1039/d4sm01311e

separated by graphene. Neither water nor oil is a good solvent for graphene or graphite due to the van der Waals forces between graphene sheets.[20] This inability to disperse graphene has, in the past, precluded its direct utilization in synthesizing conductive hydrogels. In the investigations described in this article, we use this insolubility of graphene to our advantage. We have found that placing pristine, unoxidized graphite at an oil/water interface leads to the spontaneous exfoliation of the graphite to graphene.[21] This exfoliation is driven by a lowering of the system's free energy as the graphene sheets separate the oil and water, acting much like a surfactant.[21] The insolubility of the graphene/graphite means that it is trapped at the interface and, like a surfactant, can stabilize emulsions, creating a template for polymerizing one or both emulsion phases.

Results and discussion

Exfoliation and graphene self-assembly

The ability of graphite to act as a 2D surfactant and spread (exfoliate) at oil–water interfaces provides a thermodynamically driven mechanism for the exfoliation of pristine (unoxidized) natural flake graphite to graphene.[21] These graphene sheets separate the oil and water phases, lowering the system's free energy and stabilizing water-in-oil emulsions. This creates a system of closely packed graphene-coated water droplets that form an electrically conductive network through sphere-to-sphere contact. This network was incorporated into a hydrogel by polymerizing an aqueous solution of the monomer *N*-(hydroxymethyl) acrylamide (HMA) contained in the dispersed phase of the graphene-stabilized emulsion. As illustrated in Scheme 1A, when graphite was added to a mixture of aqueous monomer solution and heptane, it was pinned at the liquid/liquid interface, with exfoliation (spreading) driven by lowering the system's free energy.[21] Emulsification of the system, shown in Scheme 1B, created additional oil/water surface area and led to additional exfoliation of the graphite to graphene.[22] Images of unpolymerized graphene-stabilized emulsions are shown in the ESI.† The graphene-stabilized emulsions were stable for at least several days, and heating led to the polymerization of the monomer in the dispersed aqueous phase. Scheme 1C illustrates the final hydrogel structure, consisting of packed graphene-coated spheres that provide a percolating conductive network throughout the hydrogel. The spheres are held together by traces of the water-soluble monomer dissolved in the hydrophobic phase and a small amount of added divinylbenzene crosslinker in the oil phase.

Effect of monomer and graphite concentration on cell size

Confocal microscopy was employed to examine the hydrogel's cell structure in its hydrated state, revealing that cell size was inversely proportional to both monomer and graphite concentrations. Higher monomer concentrations resulted in smaller spheres due to a more rapid increase in viscosity during polymerization, which stabilized the emulsion and reduced coalescence (Fig. 1A–C). Similarly, increased graphite concentration produced smaller, more numerous emulsion droplets due to enhanced interfacial stabilization from the added graphene sheets (Fig. 1D–F). These findings illustrated that monomer and graphite concentrations can fine-tune the hydrogel's cell morphology, offering control over its porosity and mechanical properties.

Emulsion templating of ECH

Although the emulsion templated the morphology of the hydrogel, it was not clear that the size of the aqueous droplets formed in the emulsion directly translated to the final material. We used acoustic spectroscopy to examine the relationship between the emulsion droplets' size and the spheres' size in the polymerized hydrogel. This technique allowed us to determine the size of the dispersed phase, even though the solutions strongly absorbed light. Fig. 2 shows the effect of increasing graphite concentration on the emulsion droplets' size with a constant monomer concentration. In Fig. 1, we observed that the spheres in the polymerized material became smaller with increased graphite loading, and the acoustic spectroscopy results supported this observation. The sphere sizes, obtained from the acoustic spectra of the emulsions, were in the size range of 80–110 μm, in line with the sizes observed by confocal microscopy in Fig. 1. Also, the lack of a significant change in the dispersity of the sphere sizes suggested that unlike with changes in monomer concentration, the change in sphere size resulting from increased graphite loading was not due to a change in the rate of coalescence but to a change in the size of the initially formed emulsion droplets.

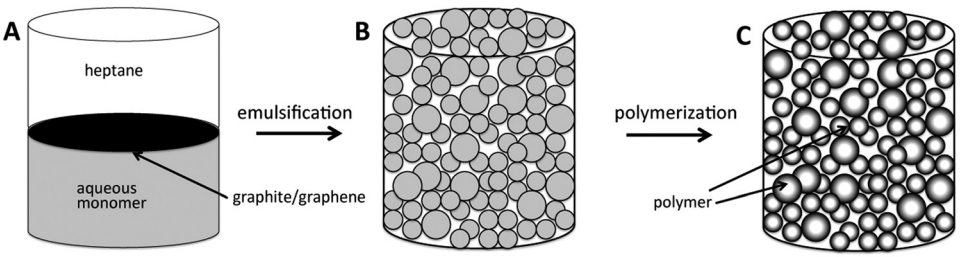

Scheme 1 Schematic describing the preparation of the conductive hydrogel. (A) Heptane, graphite, and aqueous monomer are placed in a flask. (B) Emulsifying the mixture results in aqueous drops, which are stabilized by a thin layer of overlapping graphene sheets and suspended in a continuous oil phase. (C) Subsequent monomer polymerization results in a porous, electrically conductive hydrogel after removing the oil phase by evaporation.

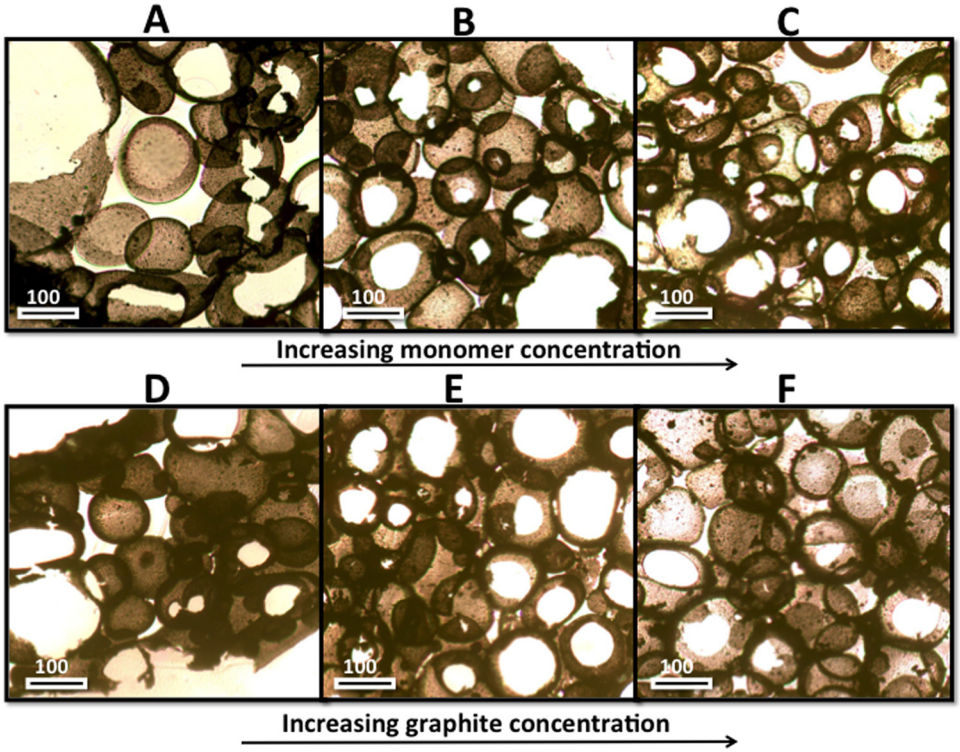

Fig. 1 Confocal microscopy images of conductive hydrogels produced from emulsions made with varying concentrations of monomer and graphite and fixed in agar for imaging. The spheres are filled with PHMA and surrounded by films of overlapping graphene sheets. The small dots are graphite particles that did not exfoliate. (A)–(C) 17.5, 20.0, and 22.5 wt% aqueous monomer solution, respectively, in emulsions containing 40 : 41: 0.60 mass ratios of water/heptane/graphite. (D)–(F) 0.45%, 0.55%, and 0.65% graphite loading relative to the total mass of the emulsion.

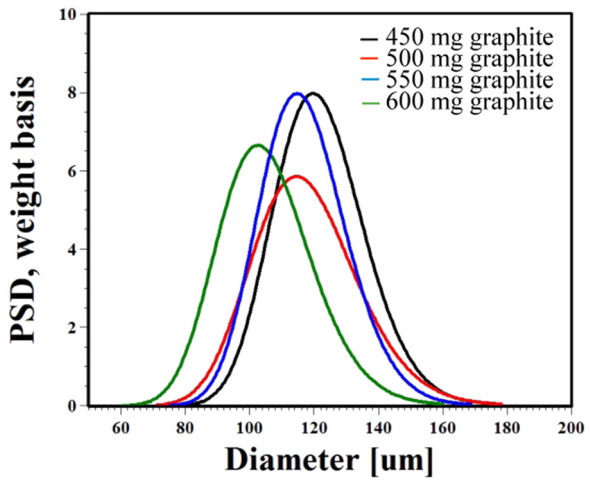

Fig. 2 Effect of graphite concentration on the size of dispersed water droplets in the graphene-stabilized emulsions. In all cases, graphite was added to 100 ml of a 2 to 3 volume ratio mixture of water and oil.

Morphology of ECH cell surfaces

While the size of the hydrogel spheres is an important parameter for controlling porosity, the morphology of the surfaces of the sphere's interior is expected to be critical for interactions with cells or chemical agents. For this, electron microscopy was used to characterize the finer structure of the spheres. Fig. 3A shows a cross-sectional FESEM image of a dried graphene/PHMA hydrogel. The imaged surface exhibits a highly porous structure with an average pore diameter between 50 and 100 μm, smaller than the spheres observed by confocal microscopy in Fig. 1 due to shrinkage of the hydrogel foam during drying. Openings, or "windows" between neighboring spheres, are visible and indicated by arrows. These windows occured at regions where the spheres touched, providing thin spots between foam cells that tear and allow bulk water to circulate throughout the hydrogel. A higher magnification image of the interior surface of a sphere, shown in Fig. 3B, shows the inside to be wrinkled after drying and shrinking, with the graphene/graphite sheets visible. In practice, dried hydrogels could be rehydrated, but the process was slow and required refluxing in

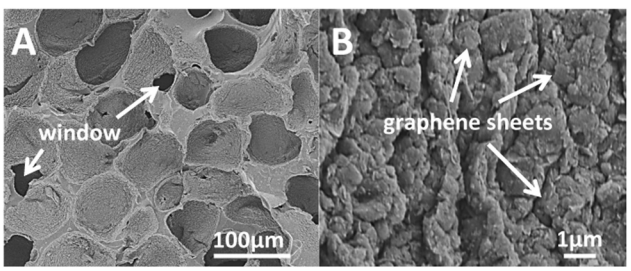

Fig. 3 Scanning electron micrograph of (A) a cross-section of a dried hydrogle composite showing windows connecting the cells of the foam. (B) Higher magnification image illustrating the graphene present on the inner walls of the foam cells.

boiling water to rehydrate in a reasonable amount of time, typically several hours.

Electrical conductivity of ECH

The percolating network of graphene sheets achieved electrical conductivities of up to 15 mS m^{-1}, a two-order magnitude increase compared to control hydrogels without emulsion templating (0.3 mS m^{-1}), as shown in Fig. 4A. This nearly two-orders of magnitude increase was due to the self-organized graphene network providing electrical percolation at low graphite loadings. Surprisingly, further increases in graphite concentration did not significantly enhance conductivity. Thermogravimetric analysis (TGA) provided insight into this phenomenon: increasing graphite loading affected the emulsion stability but did not systematically increase the final graphite content in the hydrogel (Fig. 4B).

TGA results, shown in Fig. 4B, indicated that the graphene hydrogel composites decomposed over a relatively broad temperature range. The PHMA hydroxymethyl groups decomposed between 249 °C and 277 °C. The remaining backbone decomposed between 352 °C and 383 °C, consistent with literature reports.[23] The weight loss associated with these decompositions was consistent with the chemical structure of the polymer. However, no correlation was observed between the amount of graphite used and the mass of residue in the TGA, with hydrogels synthesized with 450 mg, 550 mg, 600 mg, and 650 mg graphite showing residues of 32.2, 28.0, 30.2, 30.1, and 34.3 wt% respectively. These are the values plotted in Fig. 4A.

This lack of correlation between the amount of graphite added and the amount of residue in the TGA was due to the volume of the emulsion phase being tied to the amount of graphite added. So, while the amount of graphite added to the reaction mixtures increased from 450 mg to 650 mg, the amount of graphitic material in the final composites showed no systematic change. This discrepancy resulted from phase separation in the initial emulsion before polymerization, which created an aqueous phase covered by an emulsion phase in the final product. The polymer formed in the aqueous phase was thus not part of the conductive hydrogel. Initially, the effect of added graphite was to decrease the size of the emulsion spheres, but there was a limit to how small the sphere could be, which was related to the size of the graphene sheets.[21] Additional graphite then increased the emulsion phase's volume and thus the total amount of polymer in the emulsion phase, resulting in the wt% of graphene in the final hydrogel foam remaining reasonably constant.

ECH swelling

While increasing graphite concentration did not result in a systematic change in the electrical conductivity of the hydrogels, it did impact their swelling behavior. To determine the amount of water incorporated in the network structure as a function of time, we calculated the swelling ratios (SR) of hydrogels by using eqn (1):

$$\mathrm{SR} = \frac{M_t - M_o}{M_o} \quad (1)$$

where SR represents the average swelling ratio of a hydrogel in distilled water as measured with triplicated results, and M_t and M_o are the weights of the hydrogel at time t and the initial time, respectively. The swelling behavior of the conductive hydrogels with different amounts of added graphite is shown in Fig. 5A and B. We found that the lowest loading of graphite led to the fastest and most significant total swelling, but with increased loadings, the swelling behavior became inconsistent, mirroring the conductivity and TGA data. Taken together, these results suggest an optimal emulsion morphology, and adding more graphite simply increased the overall volume of the emulsion phase rather than changing the properties of the emulsion.

Rheology of ECHs

Turning from the graphite component to the monomer component, we found that the concentration of monomer also played a significant role in the properties of the hydrogel. Rheological analysis showed that increasing monomer concentration affected the hydrogels' elasticity and stiffness up to a limit. As shown in Fig. 6A and B, the storage modulus (G') increased with monomer concentration up to 20 wt%, beyond which further increases resulted in decreased modulus.

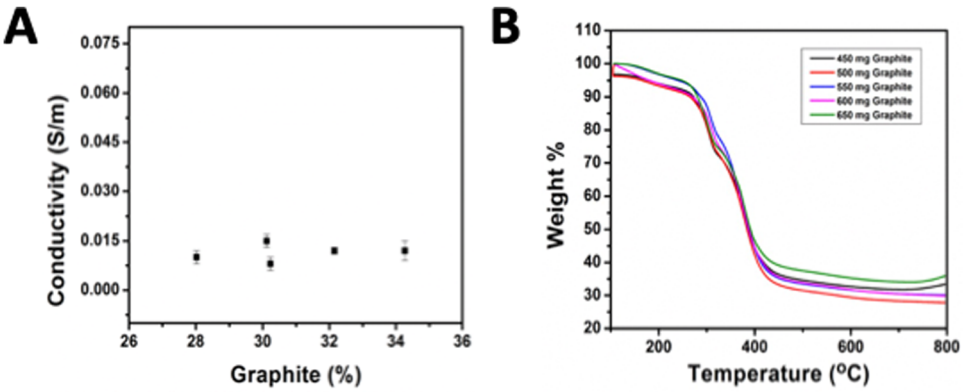

Fig. 4 (A) Effect of graphite content on electrical conductivity. Inset illustrates the approach to making conductivity measurements. (B) TGA weight loss curves for different concentrations of graphite in hydrogels.

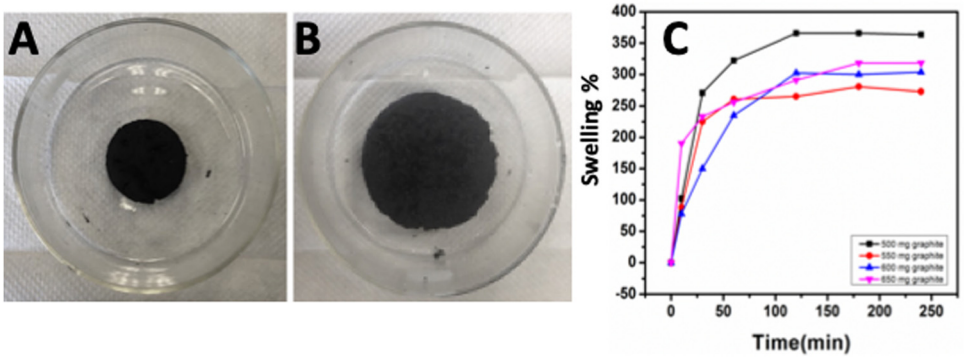

Fig. 5 Swelling behavior of conductive hydrogels (A) before placing in water (B) 15 min after placing in water (C) the swelling ratios of the conductive hydrogels immersed in deionized water (80 °C).

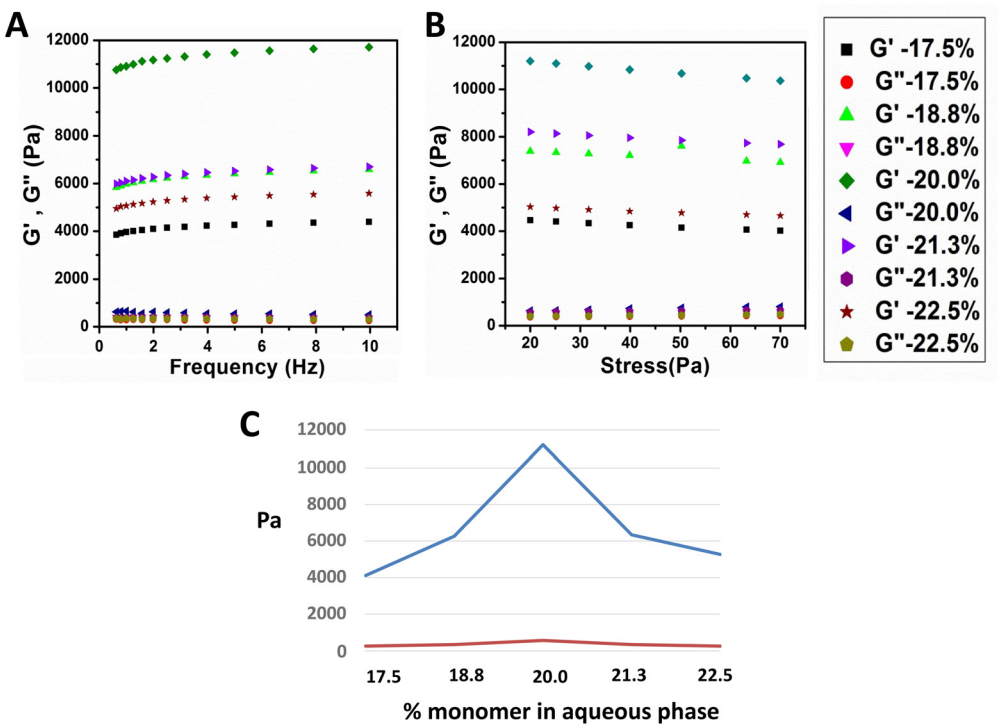

Fig. 6 Rheological behavior of hydrogels. (A) G' and G'' *vs.* frequency for hydrogels made with different monomer concentrations. (B) G' and G'' values at constant frequency (1 Hz) for hydrogels made with different monomer concentrations. (C) Comparison of G' and G'' as a function of monomer concentration, where the upper blue line is G' and lower red line is G''. Values of G' and G'' are averaged values obtained from the frequency sweep shown in (A).

Table 1 quantifies these changes in elasticity and stiffness, which are likely due to reduced interfacial tension at higher monomer concentrations (Fig. 7). This decrease in interfacial tension may have reduced the strength of the graphene network at the oil–water interface, impacting the storage modulus of the hydrogel.

The rheology of the hydrogel foams was analyzed under constant stress and temperature (25 °C) by a frequency sweep, increasing the oscillatory frequency from 0.1 to 10 Hz. As expected, and shown in Fig. 6A, in all samples, the storage modulus, G', is larger than the loss modulus, G'', since the samples are in gel states where the elastic modulus dominates. All samples also showed a broad viscoelastic region; however, the storage modulus had a maximum value at an intermediate monomer concentration. The storage modulus increased as the monomer concentration increased from 17.5 wt% to 20.0 wt% but decreased as the concentration increased past 20.0 wt%.

Table 1 Elasticity and stiffness of conductive hydrogels

Sample (wt% monomer in aqueous phase)	Elasticity (G'–G'')	Stiffness (G'/G'')
17.5	3851	14.4
18.8	5835	16.1
20.0	10 660	19.2
21.3	5951	16.3
22.5	4946	15.8

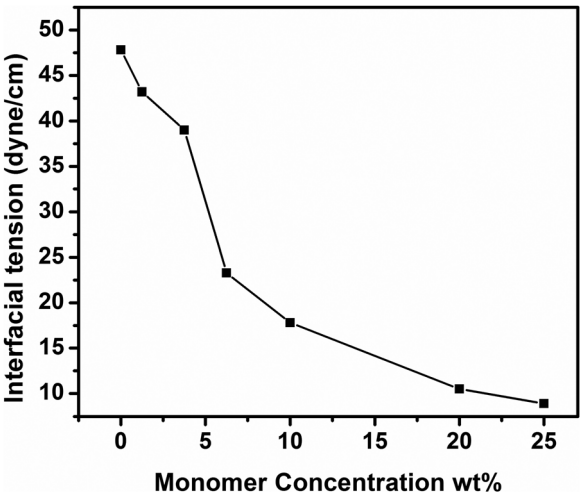

Fig. 7 Interfacial tension of aqueous monomer solution and heptane as a function of monomer concentration at 27 °C.

Table 1 shows the change in elasticity and stiffness, calculated by G'–G'' and G'/G'' respectively,[24] as the concentration of monomer used in the aqueous phase of the emulsion increased.

The increase in elasticity and stiffness as the monomer concentration increased from 17.5% to 20.0 wt% can be explained by the optical microscopy images shown in Fig. 1. The structure of the hydrogel with a 17.5% monomer concentration shows larger spheres and holes, leading to a lower elastic modulus, and a lower monomer concentration would be expected to create a softer hydrogel. However, the reason for the decrease in modulus above 20.0 wt% was not as straightforward. To understand this result, we examined the effect of the monomer on the interfacial tension between the oil and aqueous phases of the emulsion.

Interfacial tension with added monomer

Increasing the concentration of monomer changes the interfacial tension of the oil: water mixture. The ability of graphene to act as a 2D surfactant in water-in-oil emulsions depends on the large interfacial tension between the oil and water. The choice of heptane as the oil phase was based on its surface energy of 20 mN m^{-1} and its low solubility in the water phase. We measured the interfacial tension of a pure heptane/pure water interface to be 49.8 dyne per cm, which agrees with the literature.[25] We then measured the interfacial tension as the concentration of monomer in the aqueous phase increased; the results are shown in Fig. 7. We found the interfacial tension between the aqueous solution and heptane decreased with increasing monomer concentration in the aqueous phase. Lower interfacial tension reduced the driving force for graphite exfoliation and suggested a more diffuse interface. These conditions might be expected to result in less mechanically robust graphene shells and thus a smaller storage modulus. A balance between sufficient monomer concentration for mechanical integrity and preservation of high interfacial tension is therefore necessary to maintain optimal hydrogel performance.

Conclusion

In summary, we have developed a novel approach to synthesizing conductive hydrogels by leveraging the spontaneous exfoliation of graphite to graphene at an oil–water interface. This self-assembled graphene network enables electrical percolation at low graphite loadings, achieving conductivities up to 15 mS m^{-1} and structural stability, even at low filler levels. Our findings demonstrate that the mechanical and conductive properties of the hydrogels are tunable through controlled monomer and graphite concentrations, with the potential for diverse applications in advanced technologies such as bioelectronics, energy storage, and environmental monitoring. Future research will focus on optimizing the mechanical properties of these hydrogels and scaling up production to facilitate their integration into practical applications, contributing to the development of cost-effective, flexible, and conductive materials for next-generation devices.

Experimental

Synthesis

50 mg of pristine graphite (Asbury Carbon, Nano24 grade, 1 μm average flake size, >99% carbon, XRD shown in the ESI†) was first put into a 20 mL glass scintillation vial. The vial was charged with 40 μl of DVB and 6 mL *n*-heptane (Fisher Scientific, 99% Optima), followed by bath sonication for 5 min to break up any large particles (Branson 80W B2510DTH). In another flask, 1 g of *N*-(hydroxymethyl) acrylamide and 0.003 g of *N*,*N*′-methylenebis(acrylamide) were dissolved in 4 ml of water. The two solutions were mixed, and the system was tip-sonicated for 2 min to exfoliate the graphite sheets and distribute the sheets about the interface and create emulsion spheres. The emulsion was cured at 75 °C for 5 hours. Composites with different ratios of monomer and graphite were made using the same method.

Conductivity measurements

A two-point probe method using a Keithley picoammeter-voltage source (model 2420) was used to measure the electrical conductivity of the hydrated composite at room temperature. The hydrogel was embedded into two parallel copper electrodes, and then two copper wires were connected to the electrodes. Then, electrodes were connected into an electrical loop. The voltage varied from 0 to 0.01 V, and the current was measured. The volume resistivity (ρ) was calculated from the *I*–*V* curves by taking into account the geometrical characteristics of the sample:

$$\rho = R \times A/L$$

where R is the slope of the *I*–*V* curve, A is the area of the sample, and L is the distance between electrodes, corresponding to the thickness of the sample.

Electrical conductivity (σ) was calculated as the inverse of the resistivity (ρ):

$$\sigma = 1/\rho$$

Scanning electron microscopy

The composite morphology was examined by field emission scanning electron microscopy (JEOL 6335 FESEM). Samples were quickly flash frozen in liquid nitrogen, dried under a vacuum, and then coated with a thin layer of platinum ($\approx$3 nm thickness). The sample's surface was analyzed at an accelerated voltage of 5 kV.

Thermogravimetric analysis (TGA)

The composites were studied using TGA Q500 (TA Instruments) under a nitrogen atmosphere at a 10 °C min^{-1} heating rate. Before measurement, samples were dried in an oven and then ground with a mortar. Samples ranging between 10 and 30 mg in weight were added to platinum pans and heated from 25 to 800 °C.

Rheological characterization

Dynamic rheological measurements of the hydrogels are performed using an AR2000 Rheometer (TA Instruments Inc.) with a 40 mm parallel plate-plate geometry. The gap between the upper plate and the sample dish was set by moving the upper plate approximately 2 mm above the sample's surface. The upper plate was lowered very slowly (5 μm s^{-1}) while monitoring the normal force, stopping at a limit normal force of 0.1 N. After the upper plate stopped, the normal force was allowed to equilibrate to a constant value. The test methods employed were oscillatory stress sweep and frequency sweep. Operated tests recorded the storage modulus G' and the shear loss modulus G''.

Swelling measurements

The composite hydrogels were placed in excess water at 80 °C. The swelling ratio was measured by weighing the gel samples before and after hydration.

Emulsion sphere size measurements

The sphere size of the dispersed water and monomer phase was determined using a DT-1202 acoustic and electroacoustic spectrometer from Dispersion Technologies Inc. Ultrasound attenuation spectra in the frequency range from 1 to 100 MHz were analyzed with Dispersion Technology software for polydisperse emulsions to obtain the sphere size distribution.[26]

Interfacial tension

The interfacial tension of the aqueous solution/heptane was measured with a Thermo Cahn 322 Dynamic Contact Angle Analyzer (DCA).

Data availability

The data supporting this article has been included as part of the ESI.†

Conflicts of interest

The authors declare no conflicts of interest.

Acknowledgements

NSF Grants DMR-1409710 and CHE-1310453 and an AGEP GRS supplement to Grant DMR1004576 supported this work.

References

1 Y. Shi, L. Pan, B. Liu, Y. Wang, Y. Cui, Z. Bao and G. Yu, Nanostructured Conductive Polypyrrole Hydrogels as High-Performance, Flexible Supercapacitor Electrodes, *J. Mater. Chem. A*, 2014, **2**(17), 6086, DOI: 10.1039/c4ta00484a.

2 X. Tang, H. Li, Z. Du, W. Wang and H. Y. Ng, Conductive Polypyrrole Hydrogels and Carbon Nanotubes Composite as an Anode for Microbial Fuel Cells, *RSC Adv.*, 2015, **5**(63), 50968–50974, DOI: 10.1039/C5RA06064H.

3 J. Duan, H. Zhang, Q. Tang, B. He and L. Yu, Recent Advances in Critical Materials for Quantum Dot-Sensitized Solar Cells: A Review, *J. Mater. Chem. A*, 2015, **3**(34), 17497–17510, DOI: 10.1039/C5TA03280F.

4 B. Liu, P. Soares, C. Checkles, Y. Zhao and G. Yu, Three-Dimensional Hierarchical Ternary Nanostructures for High-Performance Li-Ion Battery Anodes, *Nano Lett.*, 2013, **13**(7), 3414–3419, DOI: 10.1021/nl401880v.

5 W. Zhang, P. Feng, J. Chen, Z. Sun and B. Zhao, Electrically Conductive Hydrogels for Flexible Energy Storage Systems, *Prog. Polym. Sci.*, 2019, **88**, 220–240, DOI: 10.1016/j.progpolymsci.2018.09.001.

6 T. Distler and A. R. Boccaccini, 3D Printing of Electrically Conductive Hydrogels for Tissue Engineering and Biosensors – A Review, *Acta Biomater.*, 2020, **101**, 1–13, DOI: 10.1016/j.actbio.2019.08.044.

7 N. Abu-thabit and Y. Umar Electrically Conductive Polyacrylamide-Polyaniline Superabsorbing Polymer Hydrogels. 1st International Electronic Conference on Material 2014, **1**, 1–6.

8 P. Humpolicek, V. Kasparkova, P. Saha and J. Stejskal, Biocompatibility of Polyaniline, *Synth. Met.*, 2012, **162**(7–8), 722–727, DOI: 10.1016/j.synthmet.2012.02.024.

9 M. Reynolds, L. M. Stoy, J. Sun, P. E. Opoku Amponsah, L. Li, M. Soto and S. Song, Fabrication of Sodium Trimetaphosphate-Based PEDOT:PSS Conductive Hydrogels, *Gels*, 2024, **10**(2), 115, DOI: 10.3390/gels10020115.

10 J. Hur, K. Im, S. W. Kim, J. Kim, D.-Y. Chung, T.-H. Kim, K. H. Jo, J. H. Hahn, Z. Bao, S. Hwang and N. Park, Polypyrrole/Agarose-Based Electronically Conductive and Reversibly Restorable Hydrogel, *ACS Nano*, 2014, **8**(10), 10066–10076, DOI: 10.1021/nn502704g.

11 Y. Wu, Y. X. Chen, J. Yan, D. Quinn, P. Dong, S. W. Sawyer and P. Soman, Fabrication of Conductive Gelatin Methacrylate–Polyaniline Hydrogels, *Acta Biomater.*, 2016, **33**, 122–130, DOI: 10.1016/j.actbio.2016.01.036.

12 P. R. Bidez, S. Li, A. G. Macdiarmid, E. C. Venancio, Y. Wei and P. I. Lelkes, Polyaniline, an Electroactive Polymer, Supports Adhesion and Proliferation of Cardiac Myoblasts, *J. Biomater. Sci., Polym. Ed.*, 2006, **17**(2014), 199–212, DOI: **10.1163/156856206774879180**.

13 K. Tian, J. Bae, S. E. Bakarich, C. Yang, R. D. Gately, G. M. Spinks, M. In Het Panhuis, Z. Suo and J. J. Vlassak, 3D Printing of Transparent and Conductive Heterogeneous Hydrogel–Elastomer Systems, *Adv. Mater.*, 2017, **29**(10), 1604827, DOI: **10.1002/adma.201604827**.

14 S. S. Robinson, K. W. O'Brien, H. Zhao, B. N. Peele, C. M. Larson, B. C. Mac Murray, I. M. Van Meerbeek, S. N. Dunham and R. F. Shepherd, Integrated Soft Sensors and Elastomeric Actuators for Tactile Machines with Kinesthetic Sense, *Extreme Mech. Lett.*, 2015, **5**, 47–53, DOI: **10.1016/j.eml.2015.09.005**.

15 L. Dai, *Intelligent Macromolecules for Smart Devices*, Springer London, 2004, DOI: **10.1007/b97517**.

16 M. R. Gizdavic-Nikolaidis, D. R. Stanisavljev, A. J. Easteal and Z. D. Zujovic, Microwave-Assisted Synthesis of Functionalized Polyaniline Nanostructures with Advanced Antioxidant Properties, *J. Phys. Chem. C*, 2010, **114**(44), 18790–18796, DOI: **10.1021/jp106213m**.

17 J. Lin, Q. Tang and J. Wu, The Synthesis and Electrical Conductivity of a Polyacrylamide/Cu Conducting Hydrogel, *React. Funct. Polym.*, 2007, **67**(6), 489–494, DOI: **10.1016/j.reactfunctpolym.2007.02.002**.

18 H. Pang, T. Chen, G. Zhang, B. Zeng and Z.-M. Li, An Electrically Conducting Polymer/Graphene Composite with a Very Low Percolation Threshold, *Mater. Lett.*, 2010, **64**(20), 2226–2229, DOI: **10.1016/j.matlet.2010.07.001**.

19 H. Aral and A. Vecchio-Sadus, Toxicity of Lithium to Humans and the Environment—A Literature Review, *Ecotoxicol. Environ. Saf.*, 2008, **70**(3), 349–356, DOI: **10.1016/j.ecoenv.2008.02.026**.

20 C. Cheng and D. Li, Solvated Graphenes: An Emerging Class of Functional Soft Materials, *Adv. Mater.*, 2013, **25**(1), 13–30, DOI: **10.1002/adma.201203567**.

21 S. J. Woltornist, A. J. Oyer, J. M. Y. Carrillo, A. V. Dobrynin and D. H. Adamson, Conductive Thin Films of Pristine Graphene by Solvent Interface Trapping, *ACS Nano*, 2013, **7**(8), 7062–7066, DOI: **10.1021/nn402371c**.

22 S. J. Woltornist, J. M. Y. Carrillo, T. O. Xu, A. V. Dobrynin and D. A. Adamson, Polymer/Pristine Graphene Based Composites: From Emulsions to Strong, Electrically Conducting Foams, *Macromolecules*, 2015, **48**(3), 687–693, DOI: **10.1021/ma5024236**.

23 A. Narumi, Y. Chen, M. Soné, K. Fuchise, R. Sakai, T. Satoh, Q. Duan, S. Kawaguchi and T. Kakuchi, Poly(N-Hydroxyethylacrylamide) Prepared by Atom Transfer Radical Polymewater-Solublerization as a Nonionic, Water-Soluble, and Hydrolysis-Resistant Polymer and/or Segment of Block Copolymer with a Well-Defined Molecular Weight, *Macromol. Chem. Phys.*, 2009, **210**(5), 349–358, DOI: **10.1002/macp.200800509**.

24 P. Bairi, B. Roy, P. Routh, K. Sen and A. K. Nandi, Self-Sustaining, Fluorescent and Semi-Conducting Co-Assembled Organogel of Fmoc Protected Phenylalanine with Aromatic Amines, *Soft Matter*, 2012, **8**(28), 7436, DOI: **10.1039/c2sm25673h**.

25 S. Zeppieri, J. Rodriguez and A. L. L. de Ramos, Interfacial Tension of Alkane plus Water Systems, *J. Chem. Eng. Data*, 2001, **46**(5), 1086–1088, DOI: **10.1021/je000245r**.

26 A. S. Dukhin and P. J. Goetz, *Characterization of Liquids, Nano- and Microparticulates, and Porous Bodies Using Ultrasound*, Elsevier, Oxford UK, 2010, ISSN: 1383–7303.

